JOURNAL OF APPLIED ELECTROCHEMISTRY 20 (1990) 749–755

Flow-through and flow-by porous electrodes of nickel foam
Part IV: experimental electrode potential distributions in the flow-through and in the flow-by configurations

S. LANGLOIS, F. COEURET

Laboratoire de Génie des Procédés, CNRS-ENSCR, Avenue du Général Leclerc, 35700 Rennes Beaulieu, France

Received 27 April 1989; revised 20 November 1989

Experimental distributions of the solution potential in flow-through and flow-by porous electrodes of nickel foam operating in limiting current conditions are presented. These are in good agreement with the corresponding theoretical distributions. In the case of a flow-by configuration used in a two-compartment cell, the experiments confirm the validity of the models, presented in Part III, which take into account the presence of a separator (ceramic porous diaphragm or ion exchange membrane).

Nomenclature

a_e	specific surface area per unit volume of electrode
C_0	entrance ferricyanide concentration ($y = 0$)
D	molecular diffusion coefficient of ferricyanide
E_c	cathode potential
F	Faraday number
$\bar{k}_d$	mean (and local) mass transfer coefficient
L	electrode thickness
$L_s - L$	separator thickness
m	number of sheets of foam in a stack
n	number of terms in Fourier series
Q_v	volumetric flow-rate
r_s	ohmic specific resistance of the separator
$\bar{u}$	mean flow velocity based on empty channel
V	constant potential
X	conversion
x	coordinate for the electrode thickness
y	coordinate for the electrode length
y_0	length of the porous electrode
z	number of electrons in the electrochemical reaction

Greek symbols

α	parameter $[= zF\bar{k}_d a_e C_0/\gamma_c]$
β	parameter $[= \bar{k}_d a_e/\bar{u}]$
γ	ionic electrolyte conductivity
ϕ_{sc}	solution potential in the pores of the cathode
ϕ_M	matrix potential (ϕ_M = constant)
λ	parameter $[= n\pi/y_0]$
ρ	electrolyte density
$\bar{\varepsilon}$	mean porosity
ν	kinematic viscosity
ΔE_c	potential drop in the porous cathode
$\Delta\psi$	potential drop defined in Fig. 5

Indices

c	cathodic
o	electrolyte alone
s	separator

1. Introduction

Metallic foams, which are now manufactured [1] offer interesting possibilities as materials for flow-through or flow-by porous electrodes. They are characterized by their grade (or p.p.i., number of pores per inch) and have an homogeneous nearly isotropic, very porous ($\bar{\varepsilon} \simeq 0.98$) and lightly tortuous (pore tortuosity $T = 1.3$) texture [2]. Due to their high specific surface area, a_e (about $10^4\ m^{-1}$) they perform under convective diffusional mass transfer control [3] in a manner comparable with other electrode textures such as stacks of micromesh expanded metal [4], fixed beds of spherical particles smaller than 10^{-3} m diameter [5] and other metallic [6, 7] or vitreous carbon [8, 9] reticulated structures.

Metallic foams have specific advantages for technological application: permeability, mechanical resistance, current feeding, ohmic drop through the pores [the apparent electrolyte conductivity γ in the pores is equal to the true electrolyte conductivity γ_0].

The earlier paper [10] examined the theoretical aspects of the electrode potential distribution within flow-by porous electrodes working in limiting diffusion conditions, with a special emphasis on long and thin electrodes such as can be constructed with metallic foams. The present paper deals with the measurements of experimental electrode potential distribu-

0021-891X/90 $03.00 + .12

tions within flow-through and flow-by nickel foam electrodes and with their comparison with the corresponding theoretical solutions. First, we examine the flow-through configuration and will confirm preliminary results obtained in our laboratory [11]. Second, we treat the electrode potential distributions in flow-by electrodes of a two-compartment parallelepipedic cell, the separator of which is either a ceramic porous diaphragm or an ion exchange membrane.

2. Experimental details

2.1. *General considerations*

The experimental method used for obtaining the electrode potential distribution is based on the application of the same electrochemical method as that used for mass transfer studies with nickel foam electrodes [3, 11]. Table 1 gives the electrolyte properties.

The experimental procedure makes some assumptions which agree with those made for the theoretical developments [10]:

– the porous electrode studied is a cathode where the reduction of ferricyanide to ferrocyanide under diffusion limited conditions occurs.

– in order to minimize the anodic polarization, the ferrocyanide concentration is 50 times higher than the ferricyanide concentration (see Table 1).

– the porous electrode matrix is much more conductive than the electrolyte [2] the conductivity of which, γ_0, is $20\,\Omega^{-1}\,m^{-1}$. The values of the current intensity flowing through the electrolytical circuit are small; thus, the porous electrode matrix can be considered as equipotential.

– the nickel foams studied have an almost homogeneous texture and a uniform mean porosity of about 0.98. They were previously characterized in [2].

– the presence of a supporting electrolyte (NaOH 1 N) makes the migration of the reacting ions negligible.

– the dispersion effects are negligible. Thus the flow through the stacks of nickel foam is piston-like [3].

3. Potential distribution within flow-through porous electrodes

3.1. *Experimental details*

The cell (Fig. 1) is the Altuglas cylindrical column previously used and presented in [3, 11]. This contains

Table 1. Characteristics of the electrolyte

Composition	NaOH	1 N
	$Fe(CN)_6K_4$	0.125 M
	$Fe(CN)_6K_3$	0.0025 M
Temperature	30° C	
Density	$\rho = 1.07 \times 10^3\,kg\,m^{-3}$	
Kinematic viscosity	$\nu = 1.005 \times 10^{-6}\,m^2\,s^{-1}$	
Diffusion coefficient of ferricyanide	$D = 6.4 \times 10^{-10}\,m^2\,s^{-1}$	

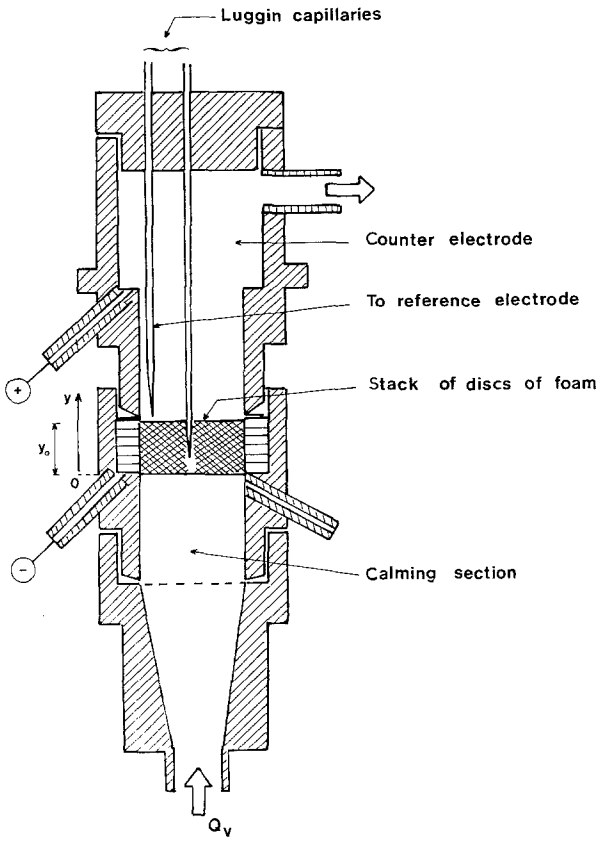

Fig. 1. View of the cell used for the study of the flow-through configuration.

the stack of m ($1 \leqslant m \leqslant 6$) circular discs of nickel foam, while the counter-electrode, located at the top of the column consists of a stack of 10 discs of grade G 100 nickel foam. The central Luggin capillary allows the local cathode potential $E_c(y) = \phi_M - \phi_{sc}(y)$ to be measured while the lateral Luggin capillary is used to fix the cathodic potential $E_c(y_0)$ at the top $y = y_0$ of the stacked electrode. Both capillaries are connected to standard reference calomel electrodes. The potential $E_c(y_0)$ is the more cathodic; its value is chosen such that all the porous cathode operates under diffusional limiting conditions.

Three nickel foams, with grades G 45; G 60 and G 100 respectively, were used for the cathodes. The height, y_0, of the stacks in the electrolyte and current flow direction was varied from 0.002 to 0.015 m. The mean electrolyte flow velocity based on the section of the empty column, $\bar{u}$, was varied between 0.002 and $0.02\,m\,s^{-1}$, a range which allows the conversion per pass, X, to be changed between 0.005 and 0.5. For an entrance ferricyanide concentration of 0.0025 M, the overall electrode potential drop, ΔE_c, measured between the bottom ($y = 0$) and the top ($y = y_0$) of the porous cathode, was varied between 0.02 V and 0.25 V.

3.2. *Comparison between theory and experiment*

The theoretical expression giving the electrode potential distribution $E_c(y) = \phi_M - \phi_{sc}(y)$ along the height of a flow-through porous electrode was verified

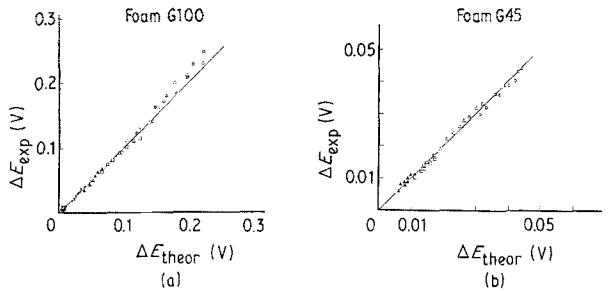

Fig. 2. Flow-through porous electrode configuration for (a) foam G 100 and (b) foam G 45: comparison between experimental and theoretical overall potential drops. No. of sheets in stack, length of porous electrode, (m, y_0): (a) ○ (6, 13.5 mm), △ (5, 11.25 mm), □ (4, 9.0 mm), ▲ (3, 6.75 mm), × (2, 4.5 mm) and ● (1, 2.25 mm); (b) ○ (6, 15 mm), △ (5, 12.5 mm), □ (4, 10 mm) and ▲ (3, 7.5 mm).

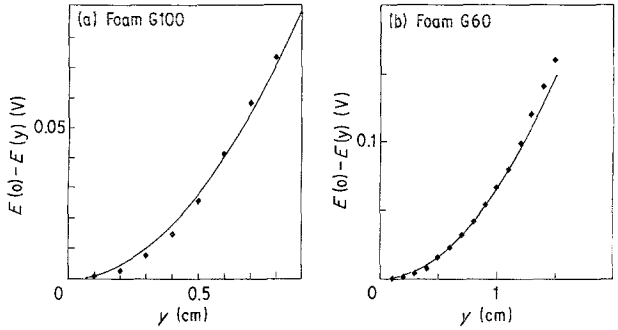

Fig. 3. Flow-through porous electrode configuration for (a) foam G 100 (4 sheets) with $\bar{u} = 1.1\,\mathrm{cm\,s^{-1}}$ and (b) foam G 60 (6 sheets) with $\bar{u} = 2.0\,\mathrm{cm\,s^{-1}}$: potential distribution along the electrode height. (——) theoretical, (◆◆◆) experimental.

by several authors in the cases of various available materials [11–14]. This expression, which was presented in different forms in the works of Sioda [15], Bennion and Newman [16], Coeuret [17], is the following:

$$E_c(0) - E_c(y) = \frac{zFC_0\bar{u}^2}{\gamma_c \bar{k}_d a_e}\left[\exp\left(-\frac{\bar{k}_d a_e y}{\bar{u}}\right) + \frac{\bar{k}_d a_e y}{\bar{u}} - 1\right] \quad (1)$$

For different stacks of nickel foam, Fig. 2 compares the experimental overall electrode potential drops, ΔE_c, to the corresponding theoretical values, that is:

$$\Delta E_c = E_c(0) - E_c(y_0) = \frac{zF}{\gamma_c} C_0 \bar{u} y_0 \left[1 + \frac{X}{\ln(1 - X)}\right] \quad (2)$$

In the application of (1) and (2), the value of the conversion, X, was calculated from the experimental limiting current, I_L. As the foams are very porous with a small tortuosity [2], the electrical conductivity, γ_c, was taken as equal to the true electrolyte conductivity, γ_0 [11].

For each category of nickel foam (G 45, G 60 or G 100), the maximum deviations between the calculated and the corresponding experimental curves are about 10%. Also, as shown in Fig. 3, there is a good agreement between the experimental electrode potential distributions and the distributions calculated from (1).

As the theoretical expressions (1) and (2) were verified for the three nickel foams, it was concluded that a systematic experimental study based on the use of several categories of nickel foam, was now unnecessary in the case of the flow-by configuration. In other words, the conclusions deduced for one nickel foam would be considered as valid for foams of other grades.

4. Potential distribution within flow-by porous electrodes

The experiments were made with a two-compartment parallelepipedic cell. Both compartments contained porous electrodes consisting of stacks of nickel foam. In order to test the approximate and rigorous theoretical models presented in [10], the separator between the two compartments was either a porous ceramic diaphragm or an ion exchange membrane. Let us recall that these models took into account the ohmic resistance of the separator and assumed as negligible the counter-electrode polarization.

4.1. *Description of the system*

The cell, made of Altuglas, is represented in Fig. 4, together with the associated flow circuit. The solution potential distributions were determined in the porous cathode (constant matrix potential, which consisted of stacks of m ($1 \leqslant m \leqslant 3$) rectangular (0.07 m wide, 0.11 m high) sheets of nickel foam. Each rectangular piece of foam was electrically soldered to a stainless steel frame (see Fig. 4c); the parts of the frame in contact with the electrolyte were painted with M-COAT D (from Vishay-Micromesures). Each cathodic stack resulted from the superposition of frames separated by flat rubber joints allowing at the same time tightness and close mechanical (and electrical) contact of the different layers of foam.

The electrolyte flowed successively through the cathodic and anodic compartments and was recycled (see Fig. 4b). The porous anode was a stack of three rectangular sheets of grade G 100 nickel foam; it was located exactly in front of the cathode in order to minimize the end current effects in the cell. Also the parts of the separator which were not in contact with the electrodes were covered with M-COAT D.

As indicated in Fig. 4a, the cover of the cathodic compartment had seven taps designed for the lateral introduction of Luggin capillaries for the solution potential determinations (taps 2 to 7) and the solution potential control near the separator at the electrode entrance (tap 1). Tap 1 and tap 2 were in the same horizontal plane while taps 2 to 7 were vertically aligned in the middle of the cell. Tap 1 was connected to a saturated calomel reference electrode; taps 2 to 7 were successively connected to another saturated calomel reference electrode.

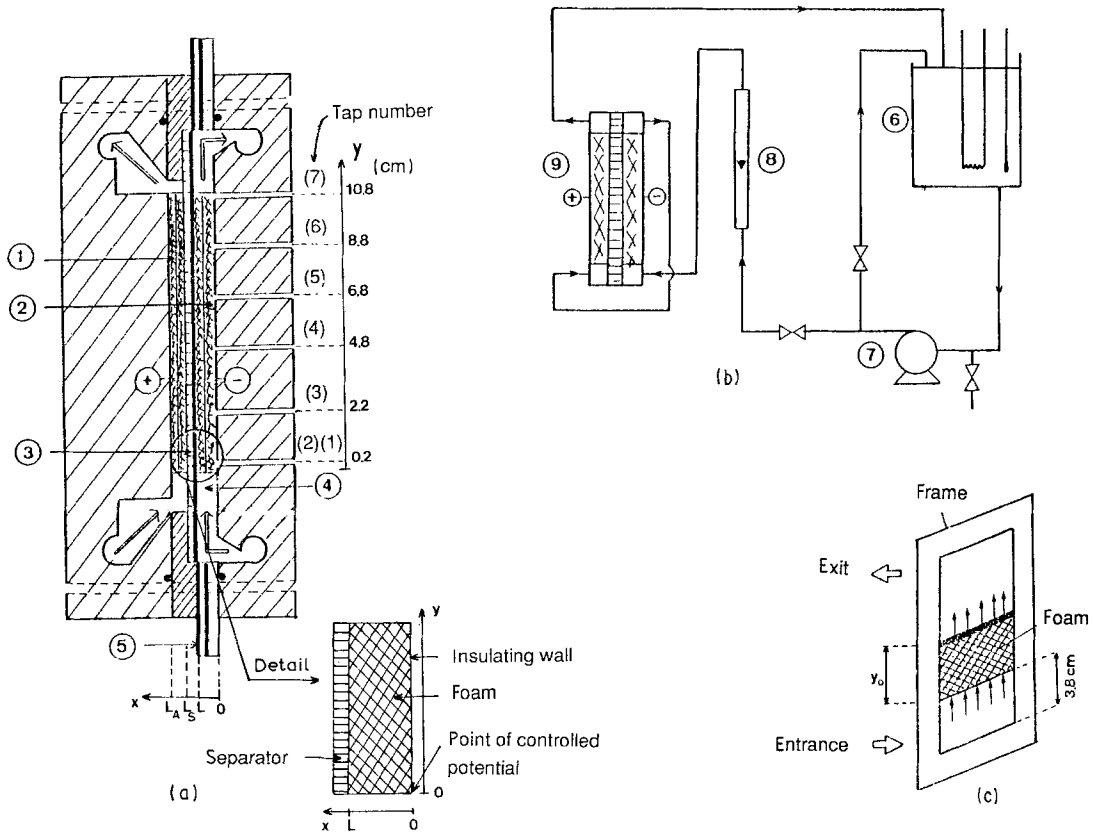

Fig. 4. Views of the cell and of the flow circuit used for the study of the flow-by configuration.
1 anode
2 cathode
3 separator
4 calming section
5 frames supporting the foams
6 reservoir
7 centrifugal pump
8 rotameter
9 cell

4.2. *Experiments via a ceramic separator*

The electrode potential distributions were determined along the height and across the thickness of a stack of sheets of grade G 60 nickel foam. The separator was a sheet of DIAPOR 8 G whose characteristics are given in Table 2; it was assumed that the porosity of this material was uniform.

The mean electrolyte flow velocity in the empty cathodic compartment, $\bar{u}$, was varied between 0.004 and 0.008 m s^{-1}. The overall limiting currents I_L measured were between 0.3 and 1.5 A; they correspond to values of the conversion per pass, X, smaller than 0.7. As the separator thickness (0.004 m) was not negligible compared to the thickness L ($0.003 \leqslant L \leqslant 0.009$ m) of the cathodic porous stacks, the experimental solution potential distributions were compared with the rigorous model presented in [10], that is with

$$\left.\begin{aligned} \phi_{sc}(x, y) - V &= \frac{\alpha}{\beta y_0}(1 - e^{-\beta y_0}) \\ &\times \left[\frac{x^2 - L^2}{2} - \frac{\gamma_c}{\gamma_s} L(L_s - L)\right] \\ &+ 2\frac{\alpha\beta}{y_0}\sum_{n=1}^{\infty}\frac{1 - (-1)^n e^{-\beta y_0}}{\lambda^2(\lambda^2 + \beta^2)} \\ &\times \left[\frac{\mathrm{ch}\,(\lambda x)}{\mathrm{ch}\,(\lambda L) + \frac{\gamma_c}{\gamma_s}\mathrm{sh}\,(\lambda L)\,\mathrm{th}\,[\lambda(L_s - L)]} - 1\right] \\ &\times \cos(\lambda y) \end{aligned}\right\} \quad (3)$$

with

$$\lambda = n\pi/y_0, \qquad \alpha = \frac{zFC_0\bar{k}_d a_e}{\gamma_c}, \qquad \beta = \bar{k}_d a_e/\bar{u}$$

In Fig. 5, the ordinate represents the values of $\Delta\psi$ which has several meanings, as indicated near the curves. The values of γ_c/γ_s which allowed the experimental potential distributions to be described by expression (3) were obtained from the comparison (see Fig. 5). In the calculations, a precision higher than 99% was obtained with 50 terms ($n = 50$) in the series

Table 2. Characteristics of the ceramic diaphragm

Commercial name	DIAPOR 8 G (Schumacher)
Thickness	4×10^{-3} m
Pore diameter	2×10^{-6} m
Porosity $\bar{\varepsilon}$	> 50%
Composition	aluminium silicate
Measured relative electrical conductivity*	3.6 in $KClO_4$ 0.01 M
	4.4 in KCl 0.01 M

*Ionic conductivity of the solution, γ_0, divided by the apparent conductivity of this solution in the separator, γ_s. The measurements were made with a cubic conductivity cell identical to that used in [4] for stacks of expanded metal.

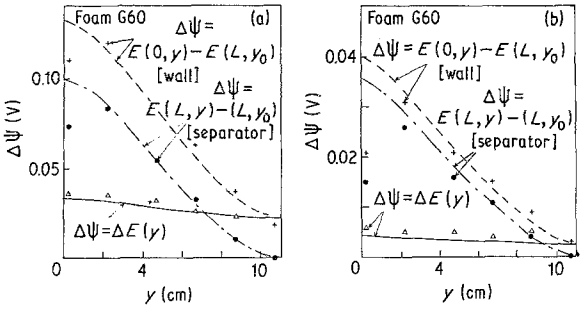

Fig. 5. Flow-by porous electrode configuration for (a) foam G 60 (3 sheets) with $\bar{u} = 1.3\,\mathrm{cm\,s^{-1}}$, $\gamma_c/\gamma_s = 11$, and for (b) foam G 60 (1 sheet) with $\bar{u} = 1.3\,\mathrm{cm\,s^{-1}}$, $\gamma_c/\gamma_s = 7$: comparisons of the experimental electrode potential distributions with Equation 3 of the rigorous model.

of (3). It is seen that both the potential distributions in the planes $x = 0$ and $x = L$, and the longitudinal potential drop across the thickness are well described by (3). Thus the rigorous model seems to apply.

It is observed that the end effects (at $y = 0$ and $y = y_0$ respectively) are small and that the separator plane ($x = L$) is not equipotential. Let us note that the local electrode potential $E_c(L, y_0)$, which is the more cathodic, is chosen as a reference in the plots of Fig. 5.

With electrode stacks made of one or two layers of nickel foam the value of γ_c/γ_s deduced from the fitting of (3) to the experimental distributions is nearly constant whatever the electrolyte velocity (see Table 3); its value of 6 (± 1) does not differ very much from the values $\gamma_0/\gamma_s = 4$ measured by conductimetry (see Table 2). In the case of three layers of nickel foam the value of γ_c/γ_s is higher than 9 and there is an increase with the flow-rate, i.e. with the current density. It is possible that the anodic polarization was not negligible during these experiments.

The potential drop across the electrode thickness, $\Delta E_c(y) = E_c(0, y) - E_c(L, y)$ is nearly independent of the value introduced for γ_c/γ_s in (3). Its value agrees with that obtained from the following expression deduced from the approximate models presented in [10]:

$$\Delta E_c(y) = \frac{zF}{\gamma_c} \bar{k}_d a_e C_0 \exp\left(-\frac{\bar{k}_d a_e y}{\bar{u}}\right) \frac{L^2}{2} \quad (4)$$

Table 3. Values of the relative conductivity γ_c/γ_s deduced for the ceramic porous diaphragm from the fitting of Equation 3 with experimental curves

Flow-rate, Q_v ($l\,h^{-1}$)	*10*	*30*	*50*
γ_c/γ_s 3 sheets of foam G 60 ($L = 0.009$ m)	9	11	13
γ_c/γ_s 2 sheets of foam G 60 ($L = 0.006$ m)	5	6	6
γ_c/γ_s 1 sheet of foam G 60 ($L = 0.003$ m)	7	6	6

Table 4. Characteristics of the cation exchange membrane

Commercial name	CMV-Sélémion
Thickness	1.5×10^{-4} m
Surfacic resistance r_s	(2 to 3.5) $\times 10^{-4}\,\Omega\,m^2$ in NaCl 0.5 M

Figure 6 shows that expression (4) is in good agreement with the experimental potential drops.

Finally, it is interesting to note in Fig. 5 that the maximum potential drop, $E_c(0, 0) - E_c(L, y_0)$, in the electrode may be 5 times higher than the potential drop across the thickness in the entrance plane, $\Delta E_c(0) = E_c(0, 0) - E_c(L, 0)$.

Thus the experimental results confirm that the influence of the separator on the potential distribution within foam electrodes cannot be neglected.

4.3. *Experiments with a cation exchange membrane*

The characteristics of the membrane are given in Table 4. By contrast with the ceramic separator, the membrane was polarisable and very thin. The nickel foam used for the construction of the porous cathodes was of grade G 100. The mean electrolyte velocity, $\bar{u}$, towards the stack of m sheets of foam ($1 \leqslant m \leqslant 3$) was varied between 0.006 and $0.1\,\mathrm{m\,s^{-1}}$. The limiting current intensity measured was between 0.4 and 2.2 A, a variation range which corresponds to conversions between 0.3 and 0.85.

As expression (3) corresponding to the rigorous model is not easily applicable to the case of membranes characterized by their specific ohmic resistance, r_s, the following expression:

$$\phi_{sc}(x, y) - V = \frac{zF}{\gamma_c} C_0 \bar{k}_d a_e \exp\left(-\frac{\bar{k}_d a_e y}{\bar{u}}\right) \times \left[\frac{x^2 - L^2}{2} - \gamma_c L r_s\right] \quad (5)$$

which was deduced from the approximate model, was used in the comparison with the experimental solution potential distributions. The values of r_s were

Table 5. Values of r_s deduced for the cation exchange membrane from the fitting of Equations 5 with the experimental results obtained in the wall plane ($x = 0$)

Flow-rate, Q_v ($l\,h^{-1}$)	*10*	*20*	*30*	*50*
r_s for 3 sheets of foam G 100 ($10^{-4}\,\Omega\,m^2$) ($L = 0.0065$ m)	5.5	–	5.0	4.5
r_s for 2 sheets of foam G 100 ($10^{-4}\,\Omega\,m^2$) ($L = 0.0044$ m)	5.5	5.5	5.5	5.0
r_s for 1 sheet of foam G 100 ($10^{-4}\,\Omega\,m^2$) ($L = 0.0021$ m)	4.5	4.5	4.5	5.0

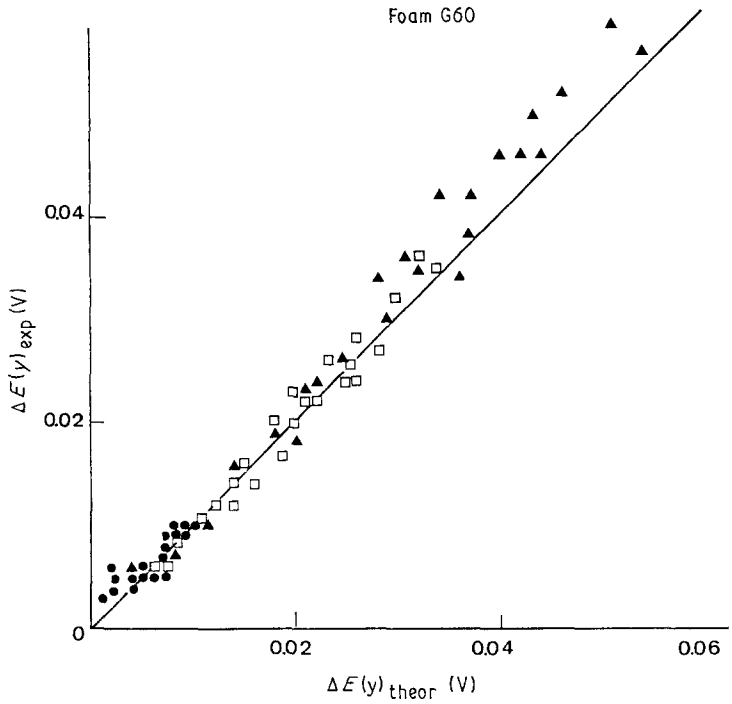

Fig. 6. Flow-by porous electrode configuration for foam G 60: comparison between theoretical and experimental overall potential drops across the electrode thickness. No. of sheets in stack, electrode thickness, (m, L): ● (1, 3 mm), □ (2, 6 mm) and ▲ (3, 9 mm).

deduced from the adjustment of (5) with the experimental distributions.

The measurements made in the plane of the wall ($x = 0$) lead to r_s values which are nearly independent of the number of sheets of foam in the stack and of the catholyte flow-rate, Q_v (see Table 5). The mean value $5 \times 10^{-4} \pm 5 \times 10^{-5}\ \Omega m^2$ of r_s is not very different from that ($3.5 \times 10^{-4}\ \Omega m^2$) given by the manufacturer. Figure 7, which summarizes the comparison for $x = 0$, takes for r_s the above value of $5 \times 10^{-4}\ \Omega m^2$. It is seen that there is a good agreement between (5) and the experimental results.

Concerning the measurements made in the plane of the membrane ($x = L$), only those made with one sheet of nickel foam ($m = 1$) led to values correctly described by expression (5). The other results were only qualitatively in agreement with the model. This is probably due to the fact that the experimental uncertainties were maximum in the plane $x = L$, for the following reasons:

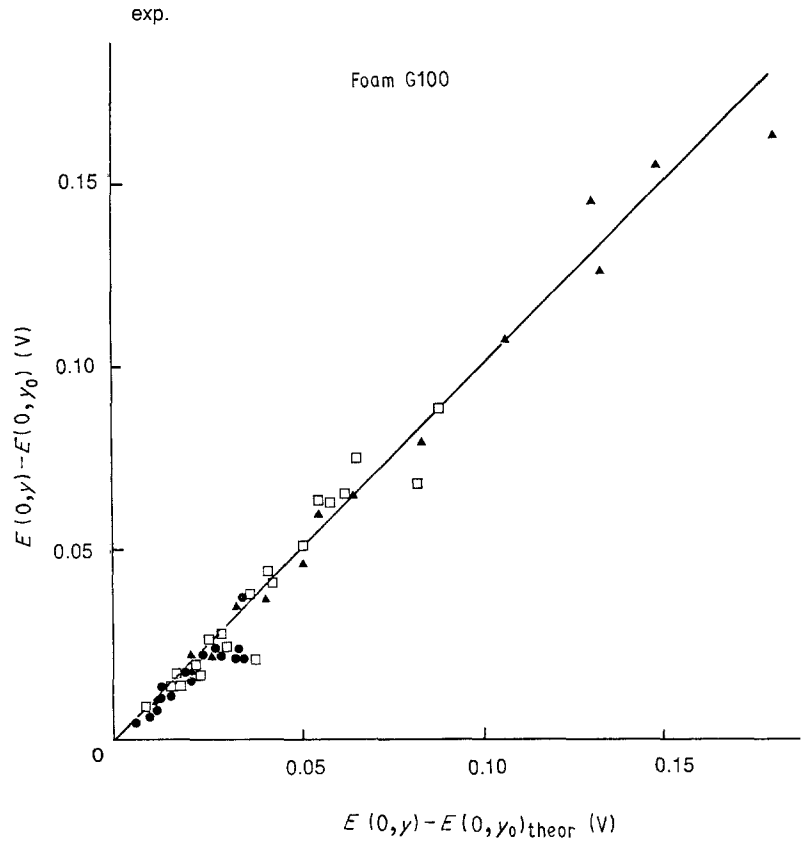

Fig. 7. Flow-by porous electrode configuration for foam G 100: comparison between experimental distributions in the plane $x = 0$ with Equation 5 of the approximate model using $r_s = 5 \times 10^{-4}\ \Omega m^2$. No. of sheets in stack, (m): ▲ (3), □ (2) and ● (1).

– the membrane does not offer mechanical resistance to the pressure exerted on it by the glass capillaries, and thus can suffer deformation.

– the slope $d\phi_{sc}/dx$ of the solution potential distribution is maximum in the plane $x = L$ (in contrast to the plane $x = 0$, at which this slope is zero, thus minimizing the effect of uncertainties in the location of the capillary).

In fact, the agreement between theory and experiment at $x = 0$ necessarily imposes a similar agreement at the membrane ($x = L$).

5. Conclusions

The experimental potential distributions confirmed the fact that the separator contributes to the uniformity of the potential distribution, as was assumed in the theoretical developments. The agreement between theory and experiment is satisfactory:

– with a ceramic porous separator the rigorous model applies

– with an ion exchange membrane the approximate model is not quantitatively sufficiently representative but there were unavoidable experimental uncertainties.

In conclusion, the design of flow-by porous electrodes made of metallic foam and working under diffusion limited conditions is possible using the approximate model presented in [10], if the counter-electrode operates at constant potential and if electrical end effects on the porous bed are minimized.

Acknowledgements

The authors thank the Direction des Etudes et Recherches d'Electricité de France for its financial support during this work and the Société SORAPEC for the free supply of the materials.

References

[1] Société SORAPEC, 94129 Fontenay-sous-Bois (France).
[2] S. Langlois and F. Coeuret, *J. Applied Electrochem.* **19** (1989) 43.
[3] *Idem, ibid.*, **19** (1989) 51.
[4] F. Leroux and F. Coeuret, *Electrochim. Acta* **30** (1985) 159.
[5] M. A. Enriquez-Granados, D. Hutin and A. Storck, *ibid.* **27** (1982) 303.
[6] A. Tentorio and U. Casolo-Ginelli, *J. Applied Electrochem.* **8** (1978) 195.
[7] D. A. Cox and R. E. W. Jansson, *ibid.* **12** (1982) 205.
[8] M. Matlosz and J. Newman, *J. Electrochem. Soc.* **133** (1986) 1850.
[9] J. Wang, *Electrochim. Acta* **26** (1981) 1721.
[10] S. Langlois and F. Coeuret, *J. Applied Electrochem.* **20** (1990) 740.
[11] J. M. Marracino, F. Coeuret and S. Langlois, *Electrochim. Acta* **32** (1987) 1303.
[12] H. Olive and G. Lacoste, *ibid.* **25** (1980) 1303.
[13] F. Leroux and F. Coeuret, *ibid.* **28** (1983) 1857.
[14] G. M. Brown and F. A. Posey, *J. Electrochem. Soc.* **128** (1981) 306.
[15] R. E. Sioda, *Electrochim. Acta* **16** (1971) 1569.
[16] D. N. Bennion and J. Newman, *J. Applied Electrochem.* **2** (1972) 113.
[17] F. Coeuret, *Electrochim. Acta* **21** (1976) 203.